

## Chapter 2

# AN ELASTIC PLATE MODEL FOR INTERSEISMIC DEFORMATION IN SUBDUCTION ZONES<sup>1</sup>

### 2.1 Introduction

At subduction plate boundaries, geodetic data from the interseismic period — decades to centuries after a megathrust earthquake — help to delineate regions of the megathrust that are not presently slipping and can potentially produce large earthquakes. Due to both observational and theoretical considerations, such data are frequently interpreted using simple elastic dislocation models (EDMs). EDMs are in fact used for interpreting secular as well as transient deformation in subduction zones [e.g., Savage, 1983; 1995; Zweck et al., 2002; Miyazaki et al., 2004; Hsu et al., 2006]. The most common of the dislocation models used for interpreting surface deformation in subduction zones is the backslip model [Savage, 1983] (henceforth referred to as the BSM, and depicted schematically in the left column of Figure 2-1). The BSM was originally motivated by the recognition that the overriding plate apparently experiences little permanent inelastic deformation on the time scales relevant to the seismic cycle (several hundred years) [see, Savage, 1983]. The BSM accomplishes this zero net strain in the overriding plate by parameterizing interseismic fault slip as normal slip, i.e., backslip, on the same patch that also slips in the reverse sense during great earthquakes [Savage, 1983]. Therefore, the seismic cycle is completely described by two equal and opposite perturbations — abrupt coseismic reverse slip cancels cumulative interseismic normal slip (or “backslip”) at the plate convergence rate. Thus, to first order, the interseismic strain field and the sum of coseismic and postseismic (afterslip) strain fields must cancel each other, and asthenospheric relaxation does not significantly contribute to the interseismic deformation field [Savage, 1983, 1995]. Further, it has been shown that the predictions of interseismic surface velocities for a two-layered elastic halfspace model (e.g., elastic-

---

<sup>1</sup> Published in JGR-Solid Earth: Kanda, R. V. S., and M. Simons (2010), An elastic plate model for interseismic deformation in subduction zones, *J. Geophys. Res.*, 115, B03405, doi:10.1029/2009JB006611.

layer-over-elastic-halfspace) differ by less than 5% from those for a homogeneous elastic-halfspace model [Savage, 1998]. Similarly, the effect of gravity on the elastic field is also very small ( $< 2\%$ , see [Wang, 2005]). In the case of linear elastic-layer-over-viscoelastic-halfspace models, data for the interseismic period do not require asthenospheric relaxation, and can be fit equally well by afterslip downdip of the locked zone in an equivalent homogeneous elastic-halfspace model [Savage, 1995].

Thus, the BSM provides a first-order description of the subduction process on the time-scale of several seismic cycles (on the order of  $10^3$  yrs) using only two parameters — the extent of the locked fault interface and the plate geometry (constant or depth—dependent fault dip). To be precise, the BSM as intended by Savage [1983], assumed a mature subduction zone — where plate bending and local isostatic effects on the overriding plate are compensated by unspecified “complex asthenospheric motions” [Savage, 1983, page 4985]. These asthenospheric motions are assumed not to play a role in surface deformation, and there is no net vertical motion between the two plates at the trench. Thus, the BSM as intended by Savage [1983] is purely a perturbation superimposed over steady state subduction, with the deformation fields due to coseismic slip (thrust sense) and cumulative post-/interseismic-slip (backslip) on the locked portion of the fault canceling each other (left column of Figure 2-1 and Figure 2-2). Therefore, the BSM does not include block motion [Savage, 1983, page 4985; and J.C. Savage (personal communication, 2009)]. Henceforth, we use BSM to refer to this original model, as intended by Savage [1983]. However, subsequent authors have interpreted the relative steady state motion illustrated in Figure 1 of Savage [1983] literally, assuming that steady state motion implies block-motion (e.g., Yoshioka et al. [1993], Zhao and Takemoto [2000]; Vergne et al. [2001]; Iio et al. [2002; , 2004]; Nishimura et al. [2004]; Chlieh et al. [2008a]). Henceforth, we use pBSM to refer to this popular (mis-) interpretation of the BSM with block-motion (middle column of Figure 2-1 and Figure 2-2). In the pBSM, the interseismic backslip perturbation applied to the locked zone is viewed as the difference between two elastic solutions: (a) continuous steady state rigid-block motion along the plate interface, and (b) continuous aseismic slip along the plate interface

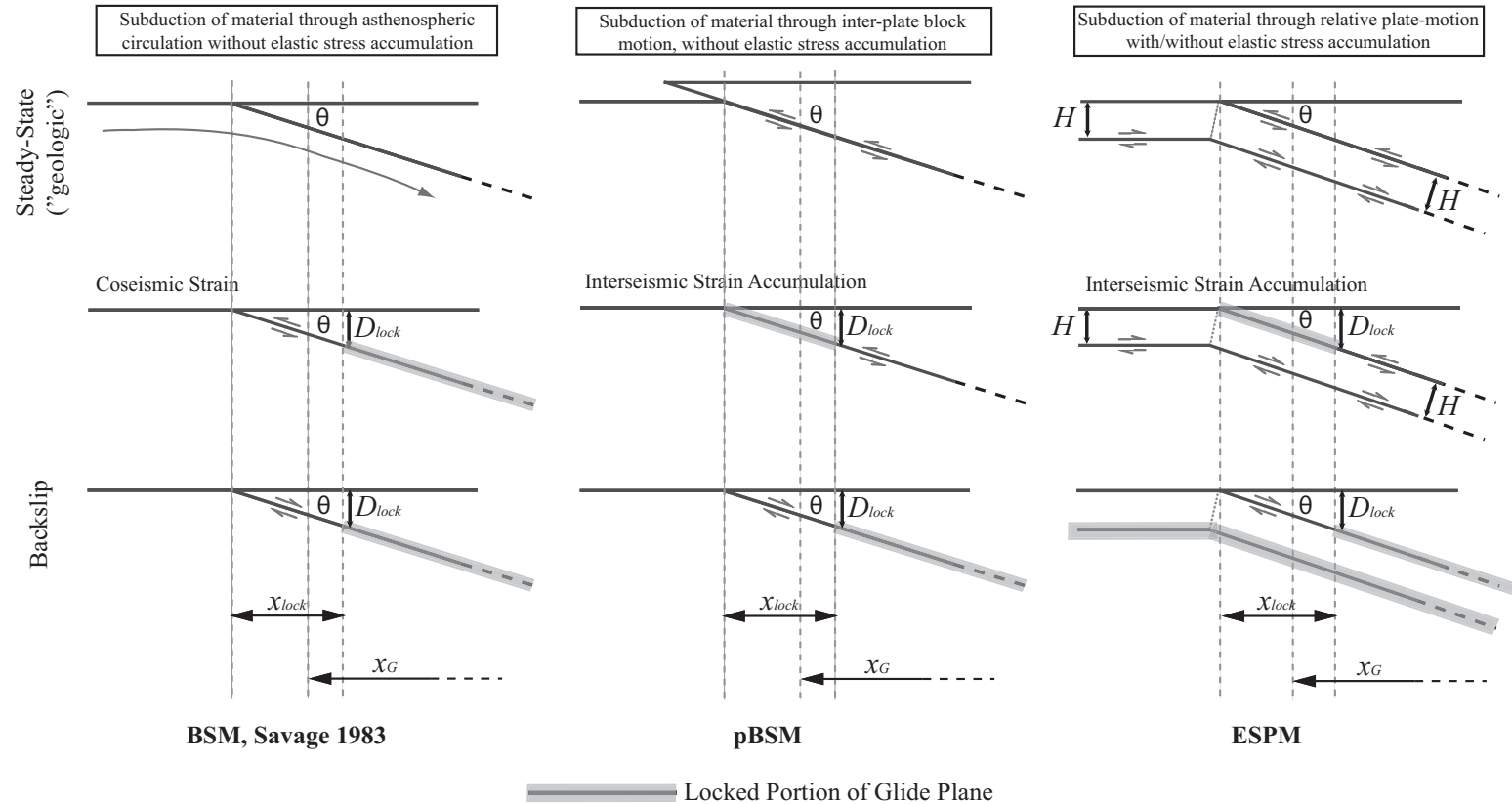


**Figure 2-1** Comparison of the BSM, the pBSM, and the ESPM. The trench is defined by the intersection of the free-surface (horizontal solid line) and the (upper) dipping line; cross-sectional geometry is assumed to be identical along strike;  $D_{lock}$  is the depth to the downdip end of the locked megathrust;  $x_{lock}$  represents the surface projection of the downdip end of the locked megathrust;  $\theta$  is the dip of the plate interface;  $H$  is the plate thickness in the ESPM;  $x_G$  represents the typical range for the location of the nearest geodetic observation from the trench. The arrows represent relative motion at the plate boundary.

downdip of the locked zone, representing the interseismic strain accumulation process. Thus, in the pBSM, the asthenosphere is primarily represented as two rigid fault blocks, and strain accumulation is assumed to occur only at the upper boundary of the subducting plate, specifically, as steady-slip downdip of the locked zone. The pBSM is unphysical in that on longer time scales, the steady state block motion along the megathrust interface between the two converging plates results in net long-term uplift of the overriding plate, as well as an unrealistic prediction of zero net strain in the downgoing plate. *Ad hoc* arguments have been used to simply ignore the vertical component of block motion, while including its horizontal component to account for plate convergence. From the perspective of implementation and interpretation, the pBSM is also ambiguous when considering non-planar faults — i.e., where one should one impose backslip. Even though the original BSM envisaged by Savage [1983] postulates application of backslip directly to the locked interface, irrespective of its geometry, this ambiguity arises in the pBSM because assuming block motion along a non-planar interface leads to net deformation in the overriding plate over the seismic cycle (upper middle panel of Figure 2-2), violating the original BSM's assumption of zero-net deformation there. As a result, several authors have either used a fictitious planar fault tangent to the downdip end of the locked zone to apply interseismic backslip [e.g., Simoes et al., 2004; Chlieh et al., 2008], or have argued against the use of the BSM for curved fault geometries [e.g., Chlieh et al., 2004].

In order to reconcile a plate view of subduction with observed deformation over the seismic cycle, we propose here a plate-like EDM for subduction zones, the ESPM, that essentially differs from the BSM as well as the pBSM in the form of the steady state solution (right column of Figure 2-1 and Figure 2-2). The steady state “plate” solution in the ESPM is simply the superposition of two parallel dislocation glide surfaces in the half-space, representing the top and bottom of the plate. The ESPM is intended to be a kinematic proxy for slab driven subduction [e.g., Forsyth and Uyeda, 1975; Hager, 1984], where the shear strains between the bottom of the downgoing plate and the surrounding mantle are approximated by the bottom dislocation glide surface. So, the

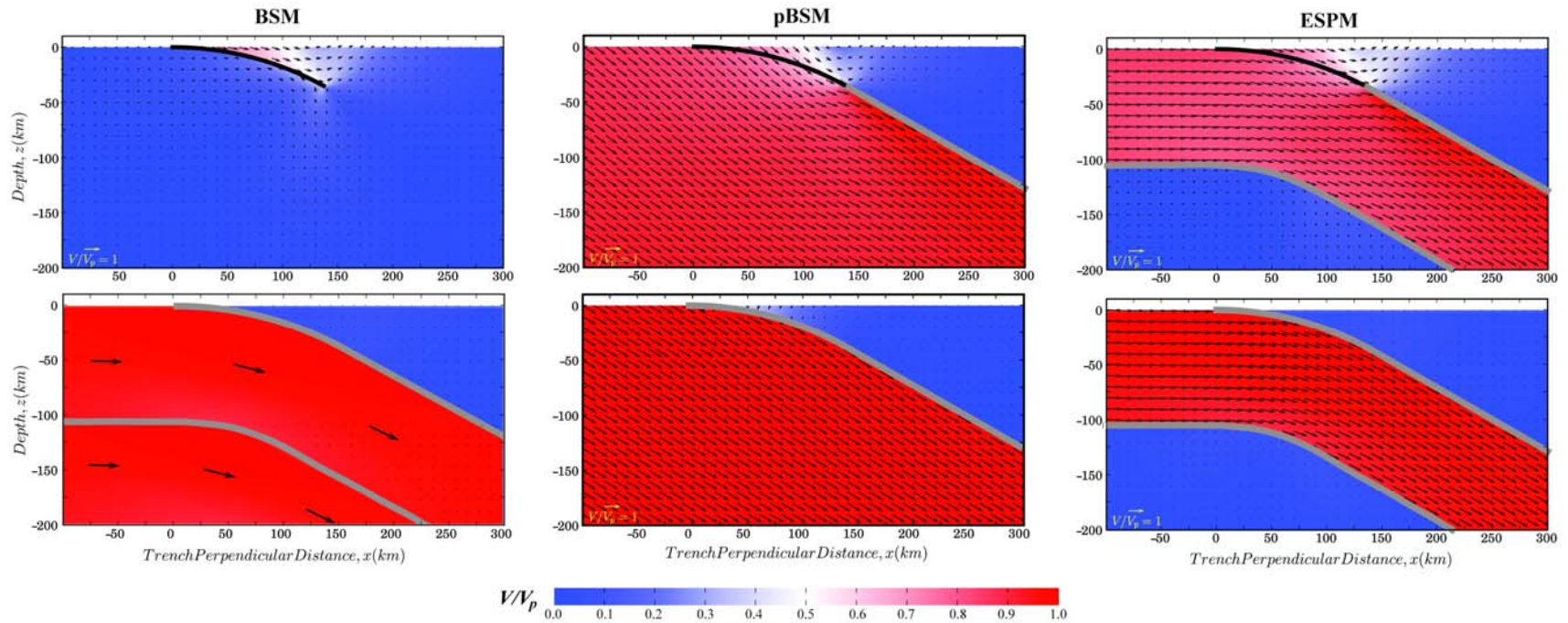


**Figure 2-2.** Comparison of the velocity fields in the half-space for the BSM, the pBSM, and the ESPM. Top row illustrates the interseismic velocity fields predicted by the models (solid black line represents the locked zone), and the bottom row shows the imposed “geologic” steady state creep velocity field. All velocities are computed relative to the far-field of the overriding plate (and normalized relative to the plate convergence rate,  $V_p$ ). Velocity vectors are drawn to the same scale in all panels (yellow vector at bottom left in each panel), relative to the plate convergence rate. The steady state field for the BSM is only a schematic representation of “complex asthenospheric motions” assumed by Savage [1983], and not a computed field.

ESPM retains the BSM's mathematical simplicity, while providing more intuition regarding the plate bending process. Because bending is explicitly included in the ESPM, the fraction of flexural stresses released continuously over the seismic cycle,  $f_{\sigma}$ , as well as plate thickness,  $H$ , are two additional parameters in this model. Our goals here are to (a) understand the contribution of flexure to such short-term surface deformation, (b) quantify the criteria under which flexural contribution to surface deformation can be ignored, as originally postulated by Savage [1983] for the BSM; and (c) obviate the need for many of the ambiguities inherent in the pBSM, the popular (mis-) interpretation of the BSM. We will show that the ESPM may not fit currently available geodetic data any better than the BSM, but its importance lies in providing additional physical insight into the complete elastic deformation field owing to plate flexure at the trench, and why a fault interface perturbation model has been so successful in approximating a more complicated geodynamic process like plate subduction over the seismic cycle timescale.

The simplicity of EDMs allows parameters such as the slip distribution on the subduction interface during different phases of the seismic cycle to be easily estimated from inversions of geodetic data. It is therefore not surprising that the BSM has been used to successfully fit geodetic observations using realistic plate interface geometries [e.g., Zweck et al., 2002; Khazaradze and Klotz, 2003; Wang et al., 2003; Suwa et al., 2006]. Clearly, as the quality of geodetic data as well as our knowledge of the 3D elastic structure improves, EDMs can be used to constrain more complicated models [e.g. Masterlark, 2003]. However, in spite of their success in fitting geodetic observations, it is important to remember that kinematic EDMs such as the ones discussed here fit the geodetic data by assuming that all of the observed deformation is due to current fault motion, ignoring any bulk relaxation processes [see Wang and Hu, 2006; see review by Wang, 2007]. Another disadvantage of purely elastic models is that they cannot model topographic evolution on time-scales longer than a few seismic cycles since they cannot accommodate monotonically increasing displacements (over geologic time) while keeping the stresses bounded. To the extent that such elastic deformation may provide the driving stresses for building permanent topography on the overriding plate, however, EDMs could be useful in guiding our intuition for models with inelastic rheologies. Using

the ESPM, we demonstrate below the potential for such net surface topographic evolution owing to elastic flexure of the subducting plate at the trench.

## 2.2 The Elastic Subducting Plate Model (ESPM)

If the negative buoyancy of subducting plates plays a significant role in mantle convection [as suggested originally by Forsyth and Uyeda, 1975; and explored for example, in Hager, 1984], then there must be shear tractions and associated shear strain between the downgoing slab (“plate”, or “lithosphere”) and the surrounding mantle (“asthenosphere”). We want to encapsulate the effect of such plate-driven subduction on the deformation at the surface of the overriding plate during the interseismic time period. In order to reconcile the BSM view of subduction along a single fault interface with that of subduction of a finite thickness plate at the trench, we propose a more physically intuitive and generalized kinematic model – the elastic subducting plate model (ESPM, right column of Figure 2-1 and Figure 2-2). The ESPM is constructed by the superposition of solutions for two edge dislocation glide surfaces in an elastic half-space that delineate the subducting plate, having a uniform plate thickness that remains unchanged as it subducts at the trench (right column of Figure 2-1). The lower dislocation glide surface is a kinematic proxy for the shear strains related to plate-buoyancy driven subduction. In fact, such a surface is the simplest way to explicitly account for Savage [1983]’s assumption of asthenospheric motions compensating for overriding plate deformation — especially for subduction zones that may not be mature, and therefore affected by plate flexure at the trench. By construction, the relative slip across the upper and lower plate surfaces of the ESPM is equal in magnitude, but opposite in sign. The principal effect of the lower glide surface (i.e., surface along which the lower edge dislocation moves) is to channel material in the “oceanic plate” into the “mantle”, relative to a reference frame that is fixed with respect to both the sub-oceanic mantle as well as the far-field of the overriding plate (right column of Figure 2-2). In contrast, while the pBSM considers steady state subduction of material down the trench via block motion (lower-middle panel of Figure 2-2), usually *ad hoc* arguments are used

to ignore the vertical component of block-motion – resulting in no net subduction of material into the mantle. The BSM does not explicitly model asthenospheric motions causing material subduction (left panel of Figure 2-1 and Figure 2-2).

There are two significant assumptions implicit in the construction of the ESPM. The first assumption is that the lithosphere-asthenosphere boundary is sharp (rather than diffuse), contrary to expectations from seismic, thermal, and rheological data. This simplification of a sharp lithosphere-asthenosphere boundary may be justified here because over the short timescales being considered here relative to mantle convection, surface deformation on the overriding plate is relatively insensitive to whether there is a gradient or step-jump in velocities across the lower boundary, as long as the same volume of material undergoes subduction. In addition to this kinematic role, the bottom dislocation glide also serves to decouple the shallow depths of the half-space (“lithosphere”) from mantle depths, so that there are negligible elastic stresses in the region of the half-space that would normally be considered to be viscous mantle. Further, such a sharp lower lithospheric boundary is commonly assumed in the parameterization of the flexural strength of oceanic lithosphere with an elastic plate thickness,  $T_e$  [Turcotte and Schubert, 2001], as well as in viscous plate models for analyzing long-term flexural stresses and dissipation in the subducting slab [Buffett, 2006]. Thus, the plate thickness defined in the ESPM could also be viewed as a way to parameterize the fraction of volumetric flexural stresses that may persist in the subducting lithosphere over the duration of a seismic cycle.

The second assumption is that over a single seismic cycle, the underlying “mantle” in the ESPM does not undergo significant motion relative to the far-field boundary of the overriding plate. The BSM as motivated by Savage [1983] assumes such motion as being part of the “complex asthenospheric motions” not included in that model. In contrast, by including block subsidence of the footwall (or block uplift of the hanging-wall), the pBSM predicts net relative vertical motion between the entire “oceanic” block (which includes the downgoing plate as well as the mantle) and the “continental” block (lower-middle panel of Figure 2-2), which is unrealistic. However, if this net relative uplift were



eliminated by an *ad hoc* correction to only the vertical velocity field of the overriding plate, then the pBSM would predict only net horizontal convergence between the footwall and the hanging-wall, but with a velocity equal to only the horizontal component of block motion. In addition, given that the pBSM assumes no net deformation in the overriding plate over the seismic cycle, there is no “sink” for this converging material — thus leading to a physically irreconcilable model that violates mass balance. In contrast, the ESPM satisfies continuity by allowing material to “subduct”, in addition to predicting the expected sense and magnitude of relative motion between the two plates to be at the plate convergence velocity. The ESPM can be viewed as the elastic component of lithospheric response over the seismic cycle timescale, and does not preclude the existence of viscous stresses at mantle depths (in a visco-elastic sense). In fact, one could add a (linear-) viscous mantle convection deformation field to the ESPM field below the subducting plate (similar to the layered models mentioned in the previous section), in order to introduce a gradient in the deformation field at the bottom boundary of that plate, as well as introduce relative motion between the sub-oceanic mantle and the overriding plate when integrated over several seismic cycles. Superposing such a field is no different from the asthenospheric motions envisaged by Savage [1983], because while such a field introduces long-term relative motion in the mantle underlying both plates, it does not affect the short-wavelength deformation field in the vicinity of the trench (upper-left panel of Figure 2-2), thereby not changing the predictions of the ESPM over the seismic cycle.

Thus, the ESPM adds only two extra degrees of freedom relative to the BSM — the plate thickness,  $H$ , and the fraction of flexural stresses released continuously,  $f_\sigma$  — while still retaining the BSM’s advantages (small number of parameters) for geodetic data inversion. The additional complexity of the ESPM due to these extra parameters is compensated by the elimination of ambiguities related to the implementation of the pBSM. By separating the subduction zone into distinct regions that undergo coseismic slip (locked megathrust along the upper surface) and interseismic slip (remainder of the plate surfaces), the ESPM unambiguously accounts for (a) the expected horizontal convergence at the plate-rate between the subducting and overriding plates, (b) a net zero

steady state vertical offset between the subducting and overriding plate (integrated over many seismic cycles), and (c) deformation due to slip along non-planar megathrust interfaces. As we will show in the next section, the ESPM can also be thought of as a more general model that reduces to the BSM under special conditions.

EDMs similar to the ESPM have been adopted in earlier papers on modeling interseismic surface deformation in subduction zones. For instance, Sieh et al. [1999] consider a tapered “bird-beak” shaped subducting plate whose thickness reduces to a point at its downdip end. Such a tapered geometry violates mass conservation within the subducting plate, given the purely elastic and homogeneous rheology assumed. Zhao and Takemoto [2000] propose a dislocation model for the subduction zone using a superposition of steady slip along a planar thrust fault downdip of the locked zone, and reverse slip along two lower glide surfaces representing the bottom of the subducting plate before and after the trench. However, they assume that the lower glide surfaces have interseismic velocities that are twice that of the upper surface and that the subducting plate thickness decreases with depth — both of which are again inconsistent with the conservation of mass within the subducting plate. In contrast, the simpler ESPM assumes a constant, depth invariant plate thickness for the downgoing plate,  $H$ , as well as identical slip velocity magnitudes along both glide surfaces at all times.

We use the 2D elastic dislocation solutions for a dip-slip fault embedded in an elastic half-space given by Freund and Barnett [1976], as corrected by Rani and Singh [1992] (see also, Tomar and Dhiman [2003] and Cohen [1999]) for computing surface velocities. To verify our code, we compared surface velocity predictions using the above formulation with those predicted by Okada [1992]’s compilation, for identical plate geometries. We choose the origin to be at the trench, the  $x$ -axis to be positive “landward” of the trench, and the  $z$ -axis to be positive upwards (so depths within the half-space are negative). Dips are positive clockwise from the positive  $x$ -axis. For the vertical surface deformation field, uplift is considered positive, and for the horizontal field, arc-ward motion is assumed positive. Although we only consider the plane strain problem here, the ESPM can be extended to 3D problems with along-strike geometry variations;

however, in this case, flexure associated with along-strike plate-interface curvature (e.g., Japan trench between northern Honshu and Hokkaido, or the Arica bend of the Peruvian/Chilean trench) may cause additional elastic deformation in the overriding plate.

### 2.3 End-member models of the ESPM

For the ESPM, subtracting the steady plate-subduction solution (top-right panel of Figure 2-1) from that for strain-accumulation during the interseismic (middle-right panel of Figure 2-1), we obtain a mathematically equivalent model for the interseismic — the BSM (bottom-right panel of Figure 2-1). Thus, the ESPM provides an alternate but kinematically more intuitive framework for deriving the BSM. Further, in the limiting case of the ESPM with zero plate thickness ( $H=0$ ), the edge dislocation representing the horizontal section of the bottom surface of the plate vanishes. Also, slip along the creeping sections of the top and bottom dipping surfaces cancel each other — except along the locked megathrust zone, where normal slip (or “backslip”) ensues, irrespective of fault geometry (bottom panels of Figure 2-3). Thus, backslip along the locked megathrust can also be understood as the slip prescribed along the bottom surface of a “thin” subducting plate, and in this limit, the ESPM is identical to the BSM as motivated by Figure 1 of *Savage* [1983] (left column of Figure 2-1). In this zero plate thickness limit, there is no net deformation in the overriding plate over the seismic cycle, irrespective of the plate interface geometry. In contrast, for the pBSM with a non-planar plate interface, since no lower plate boundary is assumed, net deformation in the overriding plate is unavoidable owing to steady state slip along a curved interface [e.g., Sato and Matsu'ura, 1988; Matsu'ura and Sato, 1989; Sato and Matsu'ura, 1992; 1993; Fukahata and Matsu'ura, 2006]). Thus, when using the BSM (or the pBSM) to invert for geodetic data in subduction zones, one is inherently assuming negligible thickness for the subducting plate, or continuous relaxation of stresses resulting from plate flexure. In this limit, kinematic consistency requires not only that the two glide surfaces (plate surfaces) in the ESPM have the same magnitude of slip, but also identical geometries.

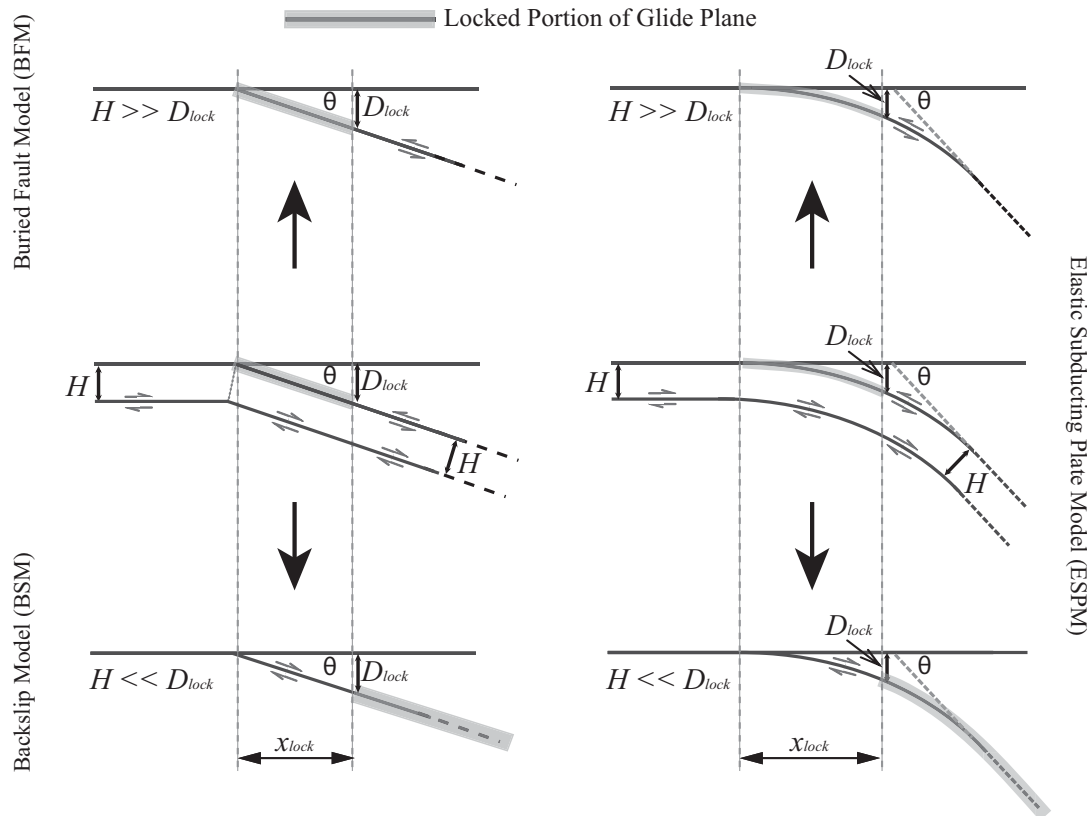


**Figure 2-3.** Geometric comparison of the ESPM with planar (left column) and curved (right column) geometry. In each column, the top row is the ESPM in the limit of a very thick plate (the BFM); the bottom row is the ESPM in the limiting case of negligible plate thickness (the BSM). Note that the “dip” of the curved fault is defined at a point where the plate straightens out. The dip of the curved fault at the trench is assumed to be zero. Other notation and assumptions are identical to those in Figure 2-1.

Therefore, when applying the pBSM to subduction zones where the downgoing slab is inferred to have a non-planar geometry, the locked megathrust interface — where backslip is imposed — should be modeled with the same geometry as that of the bottom surface of the downgoing plate directly beneath it (lower-right panel of Figure 2-3).

While there are several examples of papers that use the actual non-planar interface geometry for the BSM [e.g., Zweck et al., 2002; Khazaradze and Klotz, 2003; Wang et al., 2003; Suwa et al., 2006], some confusion has been created by the use of a planar extension of the deeper portion of a curved subduction interface for modeling backslip [e.g., Simoes et al., 2004; Chlieh et al., 2008]. Such a planar fault tangential to the interface at the downdip end of the locked zone intersects the free surface arc-ward of the

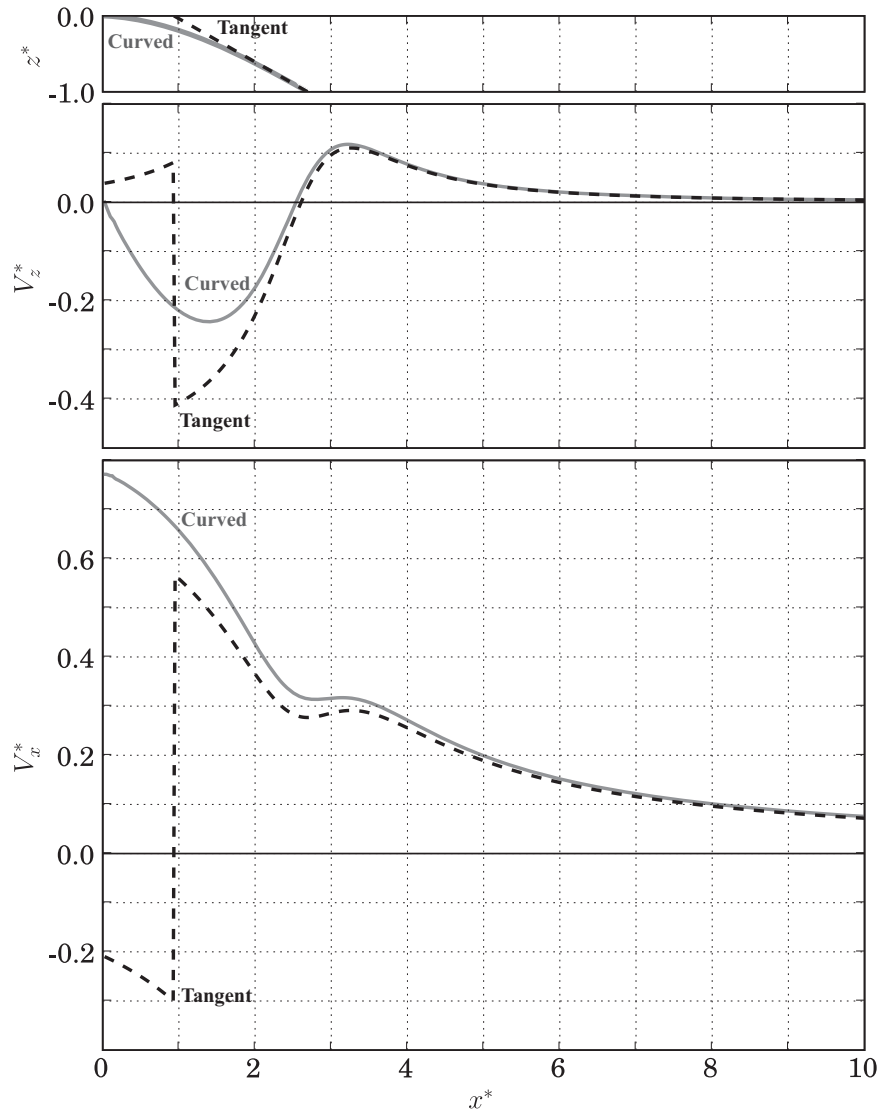


**Figure 2-4.** Appropriate application of the BSM to curved faults. Backslip must be applied to the curved interface geometry appropriate for a subduction zone, instead of to its tangent at the downdip end of the locked zone. The curved fault (solid gray line) resembles the subduction thrust interface geometry below the island of Nias, offshore of Sumatra ( $\theta_{top} = 3^\circ$ ,  $\theta_{bot} = 27^\circ$  [Hsu et al., 2006]). The tangent-approximation to the curved fault [Chlieh et al., 2004; Simoes et al., 2004; Chlieh et al., 2008] is represented by the dashed black line. The top panel presents the faults in cross-sectional view.  $x^*$  ( $= x/D_{Lock}$ ) is the dimensionless distance perpendicular to the trench;  $z^*$  ( $= z/D_{Lock}$ ) is the dimensionless depth. The origin of the dimensionless  $x^*$ - $z^*$  system is at the location of the trench axis. Vertical surface velocity profile,  $V_z^*$  (middle panel), and horizontal surface velocity profile,  $V_x^*$  (bottom panel), are scaled by the uniform plate convergence velocity,  $V_p$ .

trench (“pseudo-trench”, top panel of Figure 2-4). The surface velocity predictions in the far-field due to slip on a curved fault and its tangent planar approximation are nearly indistinguishable. But because of the artificial arc-ward shift in the tangent approximation’s “trench”, its predictions of surface deformation differ significantly from those for the curved megathrust right above the locked interface (middle and bottom panels of Figure 2-4). An additional concern is the use of entirely different faults for coseismic and interseismic displacements. Savage [1983] explicitly states this notion of applying backslip to the megathrust interface, irrespective of its shape. But as discussed earlier, that model’s application by subsequent researchers – possibly arising from the pBSM notion of block-motion - have created an apparent ambiguity in the implementation of the BSM to non-planar fault geometries.

In the limiting case of the ESPM with very large plate thickness ( $H \rightarrow \infty$ ), the lower glide surface is at a large depth below the upper plane, and for a fixed radius of curvature (typically a few hundred km), the plate behaves like a planar slab with a sharp kink at the trench (left panels of Figure 2-3). So, the contribution of the bottom glide surface reduces to a single dislocation at this kink that is deeply embedded within the half-space. Consequently, the contribution of the bottom glide surface has almost negligible amplitude and a very broad wavelength, its contribution to the total ESPM surface deformation field becomes negligible. The only contribution to the surface ESPM deformation field in this “infinite-thickness” limit comes from the buried thrust fault downdip of the locked zone. Thus, in this limit of “infinite” plate thickness (i.e., for very thick plates, as in plate collision zones), the ESPM mathematically reduces to the buried fault model (the BFM, top panels of Figure 2-3), which is typically used for modeling interseismic surface deformation in continental collision zones [e.g., Vergne et al., 2001]. The ESPM can therefore be viewed as a more general model for plate convergence zones, which reduces to previously developed models for subduction (the BSM or pBSM) or collision zones (the BFM) for limiting values of plate thickness (zero and infinity, respectively).

## 2.4 Effect of plate flexure on the ESPM surface deformation field

When the plate has non-negligible thickness,  $H$ , the ESPM and the BSM differ significantly close to the trench due to strains induced by plate flexure. The differences in the predictions of the ESPM and the BSM arise from having the same magnitude of relative slip along both surfaces of the downgoing plate, as it subducts at the trench. As a consequence, material at any cross-section of the downgoing plate moves with a uniform velocity equal to the plate-convergence rate, resulting in permanent shearing of the subducting material passing through the trench. Henceforth, we use “flexural strain” to refer to this shear-dominated strain within the elastic subducting plate as it passes through the trench. The associated “flexural stresses” cause net deformation in the overriding plate at the end of each seismic cycle. So, unless these flexural stresses (a) have negligible magnitudes (as when  $H = 0$ ), or (b) are continuously released in their entirety in the shallow portions of subduction zones, the surface velocity predictions of the ESPM differ significantly from those of the BSM above the locked megathrust interface (Figure 2-5). One might argue that this region of discrepancy in these models’ predictions lies over the forearc wedge, and therefore cannot be modeled by a purely elastic model like the ESPM. However, any excess elastic deformation predicted for this zone by the ESPM (compared to that of the BSM) can provide insight into the localization of incremental inelastic strain accumulation over multiple seismic cycles. Also, to the extent that such net seismic-cycle deformation can contribute to the long-term evolution of surface topography in the real Earth, we expect inelastic processes (such as erosion, accretion and/or sedimentation) to counter any “runaway” topographic evolution resulting from the discrepancy in these models’ predictions. In addition, the ESPM can still be used to infer the short-term elastic component of wedge deformation over the duration of a single seismic cycle, especially as ocean-bottom geodetic data become available in the near future.

To understand the strain accumulation arising from our assumption of uniform velocity for the two ESPM glide surfaces, we need only consider the steady state motion of the subducting plate (i.e., without any locked patch). Such steady state motion results in a

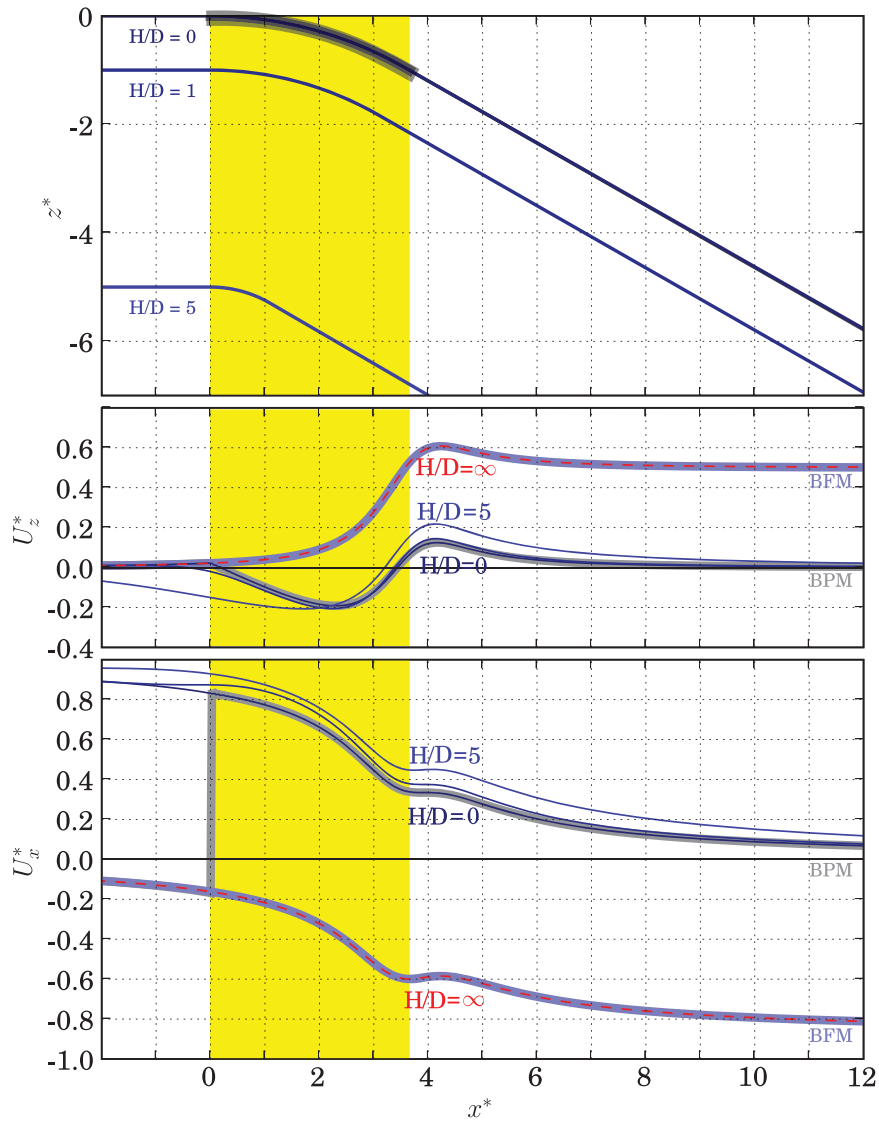


**Figure 2-5.** Comparison of deformation for the BSM and the ESPM with plates of different thickness,  $H$ , for a realistic curved fault geometry. In all panels, the thick gray solid curves represent the BSM, and the extent of the locked zone is shaded in yellow. The blue solid curve coinciding with the BSM surface velocities is the ESPM with zero plate thickness. The thick light-blue curve is the surface velocity field due to the buried thrust downdip of the locked zone (i.e., the BFM). The thin dashed red curve coinciding with the BFM surface velocity field is the ESPM having an “infinite” plate thickness. In all cases, the imposed uniform slip rate is in the normal sense for the BSM (backslip), and reverse (thrust) sense for the ESPM. Panel organization and non-dimensionalization of the plot axes is identical to that in Figure 2-4.



uniform cross-sectional velocity for material being transported within the subducting plate, and is identical to flexural shear folding, where individual layers within the plate do not undergo changes in either their thickness or length (similar to folding a deck of cards [see Suppe, 1985; Twiss and Moores, 1992]). Material moving through each layer undergoes only a change in direction as it bends through the trench during the interseismic time period (bottom-right panel of Figure 2-2). This kinematic, volume-conserving assumption leads to runaway deformation of the plate beyond the trench.

Within the framework of dislocations embedded in an elastic half-space, there are two equivalent approaches to simulating flexural stress release as the plate subducts at the trench:

- a) Applying an additional uniform velocity gradient within the plate — whose magnitude varies continuously along its length depending on the local curvature — that extends material near the top surface of the plate, and compresses material near the bottom surface as the plate subducts at the trench. This gradient is therefore zero for the planar sections of the plate before the trench and after straightening out in the upper mantle.
- b) Allowing slip at the axial hinges across which the plate successively bends as it subducts, so as to rotate planes that were perpendicular to the top and bottom surface of plate before subduction remain so after subduction.

We first consider releasing the flexural stresses in the ESPM by superimposing a velocity gradient within the plate — which is equivalent to assuming that the subducting slab behaves as a thin viscous or elastic plate in flexure [Turcotte and Schubert, 2001]. This approach is a bit arbitrary when applied to a planar interface geometry as its curvature is infinite at the trench and zero otherwise. So, we illustrate this approach using a curved plate geometry. We want plane sections that are normal to the top and bottom surface of the incoming plate to remain so as it bends through the trench and straightens out in the upper mantle. We assume that the material at the centerline (or the neutral-axis) of the incoming plate passes through the trench without a change in speed,  $V_p$ . Material above

the centerline accelerates as it passes through the trench relative to  $V_p$ , in proportion to its “radial” distance from this centerline:

$$V = \frac{V_p}{R_p} r, \quad (1)$$

where,  $R_p$  is the radius of curvature of the centerline as it passes through the bend, and  $r$  is the distance normal to the centerline profile. This would ensure that the rectangular patch in Figure 2-6(a) remains rectangular as it passes through the trench. So, the speeds for the top and bottom surfaces of the plate would be:

$$\begin{aligned} V_{top} &= \frac{V_p}{R_p} R_{top} = \frac{V_p}{R_p} \left( R_p + \frac{H}{2} \right) = V_p \left( 1 + \frac{HC_p}{2} \right) = V_p \left( 1 + \frac{\delta V}{V_p} \right) \text{ and} \\ V_{bot} &= \frac{V_p}{R_p} R_{bot} = \frac{V_p}{R_p} \left( R_p - \frac{H}{2} \right) = V_p \left( 1 - \frac{HC_p}{2} \right) = V_p \left( 1 - \frac{\delta V}{V_p} \right) \end{aligned} \quad (2)$$

where  $R_{top}$  and  $R_{bot}$  refer to the local radii of curvature for the top and bottom surfaces of the plate,  $H$  is the plate thickness, and  $C_p$  is the plate curvature.  $C_p$  is equal to zero for the straight sections in the ESPM. So, the velocity corrections apply only to the curved section of the subducting plate. For radius of curvature,  $C_p$ , equal to 250 km (which is roughly the value used for all the curved profiles in this paper), and an elastic plate thickness,  $H$ , of 50 km for the subducting lithosphere, the velocity correction,  $(\delta V/V_p)$ , equals 10%. We verified that the surface velocity field predicted by the ESPM with these velocity corrections is identical to that predicted by the BSM. Therefore, as long as the plate geometry has finite curvature, adding velocity corrections to the finite thickness ESPM ( $H > 0$ ) generates a model with no net deformation of the overriding plate (the BSM). Since the resulting surface deformation field due to this visco-elastic approximation looks identical to that for the kinematically equivalent plastic approximation (discussed next), we do not show separate plots for this approach here.

We next consider releasing flexural stresses via slip along planar axial hinges of folding as the plate subducts through the trench (the “plastic” formulation of flexure), which is equivalent to adding localized plastic deformation within the subducting plate. In order to conserve the thickness of the plate as it bends at the trench, the hinge must bisect the angle between the horizontal and bent sections of a planar subduction interface, or

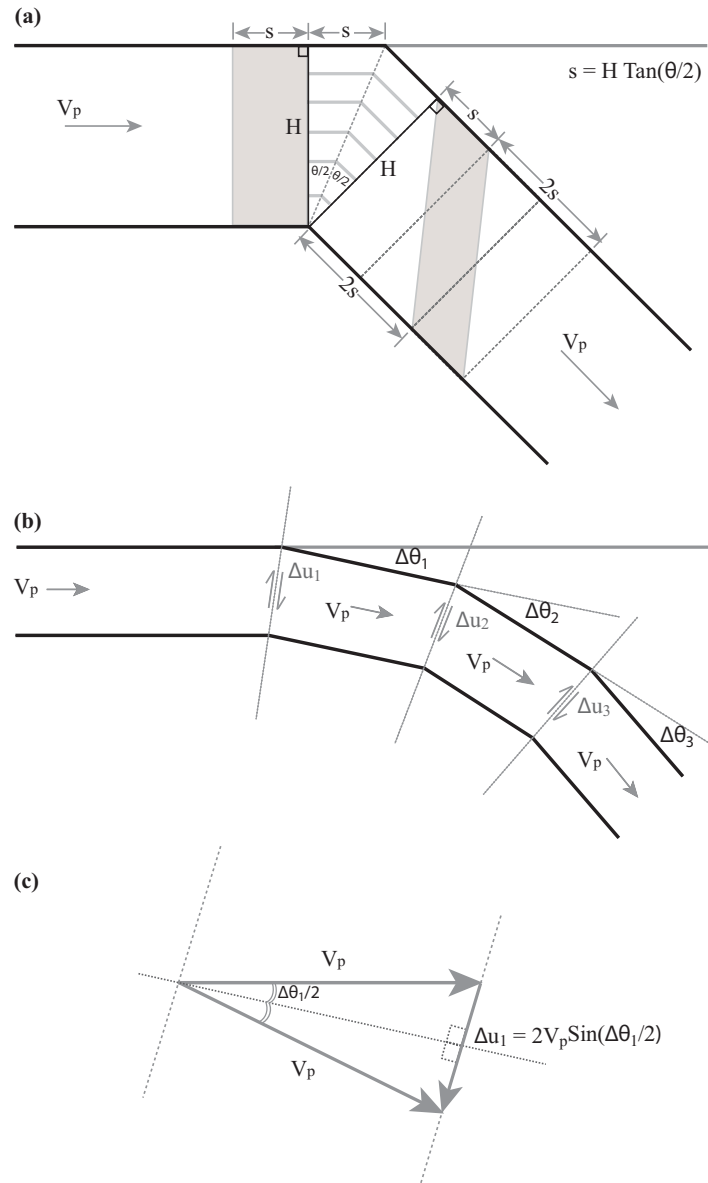


**Figure 2-6.** Kinematics of plate bending. (a) Bending of the plate at the trench for the ESPM with linear fault interface geometry; Motion of subducting material through the trench results in shearing as indicated by the shaded area. Axial hinges of folding can be kinematically represented by dislocations, across which incoming material in the plate experiences a change in direction, but not in magnitude. (b) Bending of the plate at the trench for the ESPM with a non-planar (or curved) fault interface geometry. The curved interface is represented by a number of linear segments having different slopes, and the number of hinges corresponds to the number of planar segments representing the discretization. (c) Velocity vector diagram showing required slip rate on an axial hinge to kinematically restore strains due to bending at the hinge.

between adjacent sections of a non-planar interface, whose dip changes with increasing depth (Figure 2-6(a) and (b)). Although the axial hinge plane does not experience relative displacement across itself, it can be shown that the deformation gradient tensor associated with this plane is identical to that of a fault experiencing relative displacement across that plane, especially at distances larger than the radius of curvature of the fold hinge [Souter and Hager, 1997]. A curved fault can be thought of as bending along a set of such axial hinge planes, whose number depends on the discretization of the non-planar fault profile (Figure 2-6(b)). As the discretization of the fault profile becomes finer, correspondingly more hinges are required to accurately model flexural strains. Axial hinges help relax the accumulated flexural stresses by allowing the transport of material from the vicinity of the trench down the subducting plate in a kinematically consistent way (Figure 2-6(c)) – resulting in a thrust sense of slip across each axial hinge with the magnitude,

$$\Delta v = 2V_p \sin\left(\frac{\Delta\theta}{2}\right), \quad (3)$$

where,  $\Delta v$  is the relative slip required to exactly compensate for plate flexural strains at the hinge, and  $\Delta\theta$  is the same as in Equation 1. Again, in the limiting case of a curved fault, this reduces to,

$$\Delta v \approx V_p \Delta\theta. \quad (4)$$

Figure 2-6(a) geometrically illustrates this flexural strain for a planar fault interface characterized by a single discrete bend in the subduction plate. Since the two glide surfaces have the same slip rate, the gray rectangular volume in that figure is sheared into a parallelogram after completely passing through the trench. The accumulated shear strain due to bending (represented by the hachured zone in Figure 2-6(a)) is proportional to the difference in path lengths for the top and bottom edges of the rectangle at the upper and lower dislocations (Figure 2-6(a)):

$$\varepsilon_{xz} = \frac{2H \tan(\frac{\Delta\theta}{2})}{H} = 2 \tan(\frac{\Delta\theta}{2}), \quad (5)$$

where  $\varepsilon_{xz}$  is the shear strain, and  $\Delta\theta$  is the change in dip angle at the trench. Similarly, a curved geometry can be thought of as a series of infinitesimally small bends in the plate (Figure 2-6(b)). In this case, the incremental strain due to each such bend can be calculated from Equation 1, in the limit of infinitesimally small  $\Delta\theta$ .

$$\Delta\varepsilon_{xz} \approx 2(\frac{\Delta\theta}{2}) = \Delta\theta, \quad (6)$$

which is identical to pure shear. In this case, the local rate of strain accumulation along the curved plate is given by:

$$\frac{d\varepsilon_{xz}}{dt} = V_p \left. \frac{\Delta\varepsilon_{xz}}{\Delta s} \right|_{\Delta s \rightarrow 0} = V_p \left. \frac{\Delta\theta}{\Delta s} \right|_{\Delta s \rightarrow 0} = V_p C_p, \quad (7)$$

where  $V_p$  is the long-term plate convergence velocity,  $t$  is time,  $s$  is the arc-length along the curved profile, and  $C_p$  is the local curvature of the profile, as in Equation 2. So, the strain rate in the slab is proportional to the convergence velocity and curvature in this purely kinematic model. Because this derivation was based on fixing the geometry of the plate, the strain rate obtained above is equivalent to that derived for viscous plates by Buffett [2006], or bending of thin plates by Turcotte and Schubert [2001], except for a factor of distance from neutral axis (since we have assumed uniform velocity here).

Henceforth, we use “flexural field” to denote the deformation field resulting from either the velocity corrections or the axial hinges for a steadily slipping plate with no locked zone on the subduction thrust interface (Figure 2-7(a) and Figure 2-8(a)). Subtracting the surface velocity field due to either of the flexural fields from that for the ESPM having a locked zone results in the BSM surface velocity field (Figure 2-7(b) and Figure 2-8(b)). It is important to note that the plate interface geometry has a very strong effect on the shapes of the surface velocity profiles of the flexural field. For the planar interface, both the horizontal and vertical surface velocity profiles indicate that the frontal wedge of the

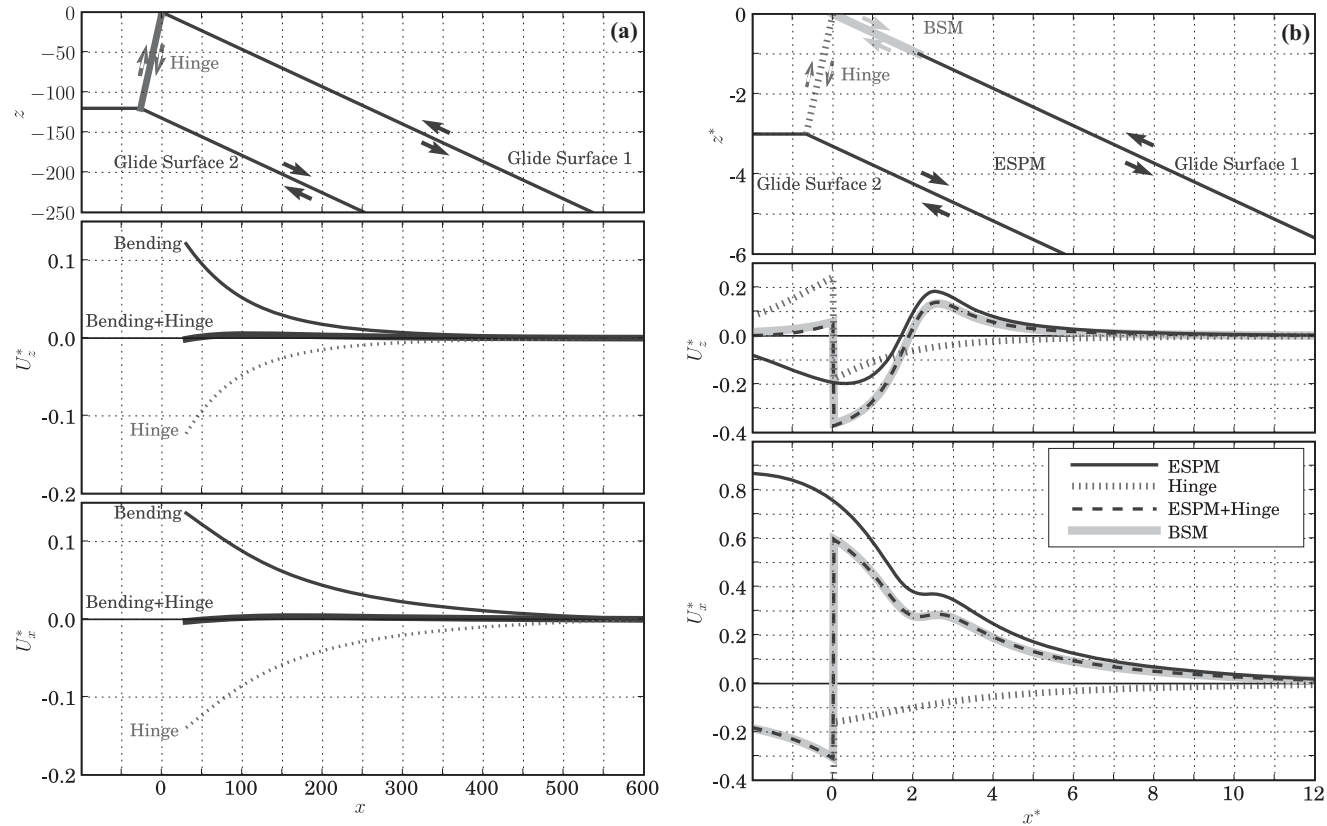


**Figure 2-7.** The surface deformation field for the ESPM for a planar plate geometry: (a) the ESPM with no locked zone is equivalent to the long-term, steady state plate motion (solid black line). The surface velocity field due to the axial hinge (thin dashed gray line) cancels the effect of plate flexure at the trench (thin solid black line), resulting in net zero long-term strain accumulation over the seismic cycle (thick solid black line). (b) Effect of a single axial hinge on the ESPM with a locked megathrust fault. Again, note that the ESPM predicts the correct sense of motion for the oceanic plate. The sum of the ESPM (thin solid black line) and axial hinge (thick dotted gray line) velocity fields — shown as the thick dashed black line — exactly equals that for the equivalent BSM (thick solid gray line). Panels and plot axes are as described in Figure 2-4.

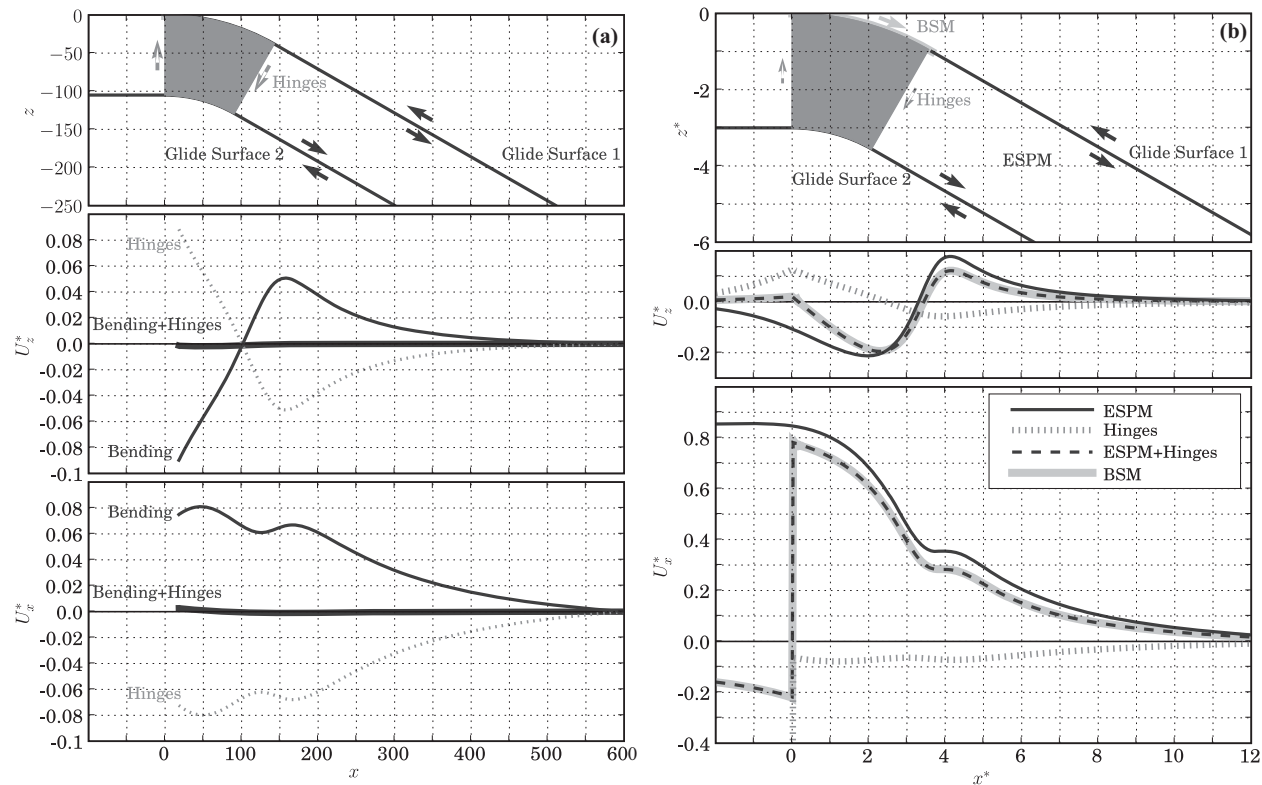


**Figure 2-8.** Surface deformation field for the ESPM for curved plate geometry: (a) the ESPM with no locked zone is equivalent to the long-term, steady state plate motion (solid black line). The axial hinges or velocity gradient corrections are introduced at positions corresponding to the discretization resolution of the curved fault. The surface velocity field due to axial hinges or a velocity gradient (thin dashed gray line) cancels the effect of plate flexure at the trench (thin solid black line), resulting in net zero long-term strain accumulation over the seismic cycle (thick solid black line). Note that the peak uplift due to the bending of a curved plate is shifted arc-ward in comparison to the peak for the planar geometry (Figure 2-7). (b) Effect of the plate flexural field (axial hinges or velocity gradient corrections) on the ESPM with a locked megathrust fault. The sum of the ESPM (thin solid black line) and axial hinge (thick dotted gray line) velocity fields — shown as the thick dashed black line — exactly equals that for the equivalent BSM (thick solid gray line). Panels and plot axes are as described in Figure 2-4.

overriding plate — immediately adjacent to the trench — undergoes net compression (bottom two panels of Figure 2-7(a)). The horizontal surface velocity profile for the curved interface is “ramp-like” — but shows more subdued strain rates (flatter slope) near the trench compared to the planar case (bottom panel of Figure 2-8(a)). In contrast, the vertical surface velocity profile for the curved interface predicts subsidence adjacent to the trench, strains having the opposite sense to those for the planar case (middle panel of Figure 2-8(a)), and attains a maximum value directly above the straightening of the plate interface at depth (compare the top and middle panels of Figure 2-8(a)).

Thus, irrespective of the geometry of the downgoing plate, adding either flexural deformation field to that for the finite thickness ESPM ( $H > 0$ , and having a locked zone) yields predictions identical to that for the ESPM with  $H = 0$  (i.e., the BSM). This equivalence between the ESPM having a finite plate thickness ( $H \neq 0$ ) and the BSM implies that if the “volumetric” flexural stresses are released continuously and aseismically in the shallow parts of the subduction zone during the interseismic period, then the surface deformation due to both BSM and the ESPM are identical for any plate thickness and shape (curvature). If these stresses are released in the deeper parts of the subduction zone (depth  $\gg H$ ) — episodically or continuously — we expect net surface topography to persist after each cycle. But in the real Earth, we would expect such topographic buildup to be modulated by gravity and limited by processes like accretion, sedimentation, and/or erosion in the frontal wedge of the overriding plate. In this equilibrium scenario, the support for near-trench flexural stresses would eventually generate surface topography that is stable after each seismic cycle. So, even when flexural stresses are released at depths ( $> 100$  km), the interseismic velocity fields from the ESPM and the BSM should be nearly identical. In all the above cases, it is appropriate to use the BSM as a simple mathematical approximation to the ESPM. However, within the context of an elastic Earth, the ESPM is still the kinematically more realistic model to interpret the pBSM. The only scenario where the ESPM and the BSM (or pBSM) surface velocity predictions differ would be when part or all of the flexural stresses not released continuously in the shallow parts of the subduction zone (e.g.,



normal faulting in the forebulge of the subducting plate) — and in this case, it is more appropriate to adopt the ESPM.

## 2.5 Comparison of the ESPM and the BSM surface displacements

As noted in the previous section, Flexural stresses near the trench cause the ESPM field to be more compressive than the BSM stress field — resulting in larger surface uplift rates above the downdip end of the locked megathrust interface. This compression is enhanced with either increasing plate thickness or plate curvature. For typical  $H/D_{lock}$  ratios and curvatures found in most subduction zones, a measurable difference exists between the BSM and the ESPM surface velocity fields ( $> 5$  mm/yr, for a typical subducting plate velocity of 5 cm/yr) up to a distance of approximately five to six times the locking depth (Figure 2-5). Intuitively, we expect that in the real Earth, the tip of the frontal wedge adjacent to the trench may not deform in a purely elastic manner. But even in this region, deformation predicted by the ESPM can be considered as the purely elastic component of the total deformation field within the overriding plate during a seismic cycle, and as the driving force for inelastic deformation — and the discrepancy between the ESPM and the BSM (or the pBSM) at a horizontal distance of one interseismic locking depth from the trench can still be as large as  $\sim 100\%$  in the verticals and  $\sim 15\%$  in the horizontals.

As plate thickness increases, this zone of significant difference between these two models broadens for both horizontals and verticals. The location of the zero vertical velocity (commonly referred to as the “hingeline”) for a thick plate shifts trenchward by as much as 20% from its location for the BSM (middle panel of Figure 2-5). However, the locations of the peak in vertical velocity profile or the break in slope of the horizontal velocity profile show negligible dependence on plate thickness. Increasing plate thickness results in a nearly uniform increase in the horizontal strain-rate profile, resulting in a long-wavelength upward tilt of the horizontal surface velocity field relative to the far-field boundary of the overriding plate (middle and bottom panels of Figure

2-5). Thus, a larger plate thickness enhances the non-uniform differences between the vertical surface velocity profiles of the ESPM and the BSM, in contrast to causing only a subtle change in slope between their horizontal surface velocity profiles. Therefore, vertical surface velocities are the key to differentiating between the ESPM and the BSM — i.e., for estimating the minimum elastic plate thickness for a given subduction interface geometry. Owing to the sensitivity of hingeline location to plate thickness, vertical velocities are clearly important in constraining the arc-ward extent of the locked megathrust.

Hence, to characterize both the degree of coupling and minimum elastic plate thickness, it is best to use both horizontal and vertical velocity data for geodetic inversions. Perhaps most importantly, the uncertainties in the measured vertical velocities on land must be small ( $< 1$  cm/yr) — which is possible with current processing methods for regions having good geodetic data coverage over long periods of time (e.g.,  $> 13$  years of continuous GPS coverage in Japan) — and/or ocean bottom geodetic surveys are required. Of course, we must also be confident that these vertical velocities are only due to elastic processes, and not due to inelastic effects like subduction erosion [Heki, 2004]. Therefore, given the current uncertainty of geodetic data and their location with respect to the trench, unless a thick lithosphere or a shallow locking depth can be inferred from other kinds of data (e.g. seismicity, gravity signature associated with plate flexure, seismic reflection, etc.), the BSM is as good a model as the ESPM. But the ESPM still provides not only a generalized framework for deriving, implementing, and interpreting the BSM, but also a fundamental understanding of why the BSM (or pBSM) has been so successful in interpreting interseismic geodetic data in subduction zones. This generality is an important feature of the ESPM, regardless of whether geodetic data can, at present, distinguish the predictions of this model from that of either the BSM or the BFM.

## 2.6 Elastic stresses and strains in the half-space

Subduction is ultimately governed by the negative buoyancy of the downgoing slab [e.g., Elsasser, 1971; Forsyth and Uyeda, 1975]. The kinematic assumptions used here assume that the dynamics of subduction do not change significantly during time-scales relevant to seismic cycles ( $< 10^4$  yr), and therefore the convergence velocity between the subducting and overriding plates, and the geometry of the subduction interface are relatively constant over this time period.

Viewing the BSM (or pBSM) as an end-member model of the ESPM clarifies some of the concerns of Douglass and Buffett [1995; 1996] regarding the former model. By definition, all glide surfaces in the ESPM creep aseismically (at a steady rate) during the interseismic period, continuously loading the locked megathrust as well as surrounding regions in the overriding plate. The burgers vector — which is the displacement of the edge-dislocation representing the bottom of the locked fault over one seismic cycle — accumulates steadily over the glide surfaces bounding the plate until a megathrust event. Therefore, the ESPM provides a natural explanation for the slip-rate dependence of stress along the locked zone even though there is no relative slip across that portion of the interface. It must be noted that both the BSM and the pBSM also consider the locked zone to be at rest during the entire inter-seismic period because of the superposition of steady-creep and backslip on the fault. In fact, as noted earlier, in the ESPM view of the BSM, “backslip” is actually the creep along the bottom surface of the plate, as well as equal to the creep directly downdip of the locked zone.

Another concern of Douglass and Buffett [1995; 1996] was that given the boundaries of the half-space are at infinite distance in EDMs, the tractions along the bottom of the overriding plate (“hanging-wall”) are equal but opposite in sense, on either side of the dislocation tip (i.e., the downdip end of the locked zone). Within the kinematic context of EDMs, we can make a rough estimate of the strain (and stress) perturbations introduced by BSM during a seismic cycle. Typical plate convergence rates are of the order of cm/yr with the maximum convergence having a value of the order of 10 cm/yr

( $10^{-1}$  m/yr). This long-term slip velocity divided by the typical width of the locked patch of the order of 100 km ( $10^5$  m) should give us an estimate of the magnitude of strains and stresses in the elastic half-space owing to the presence of the edge dislocation representing the locked patch. The above calculations yield a typical strain-rate of several  $\mu$ -strain/yr, which, when multiplied by a typical value of shear modulus for crustal rocks (10s of GPa), gives stress rates of the order of 10 kPa/yr. Thus, over a typical megathrust earthquake recurrence interval of 300 yrs, the accumulated stress on the locked patch reaches 3 MPa, equivalent to the average stress drop in inter-plate earthquakes [Kanamori and Anderson, 1975]. In addition to the BSM strain field, the ESPM introduces additional strains associated with material transport down the subducting plate. Observations and theoretical estimates constrain the radius of curvature for subducting plates to  $\sim 200$  km [Conrad and Hager, 1999, and references therein]. From Equation 3, we can calculate the additional flexural strain rate introduced by the ESPM to be of the order of  $0.1 \mu$ -strain/yr, ( $1/10^{\text{th}}$  of the BSM's interseismic strain accumulation rate) which causes a mean surface velocity perturbation of roughly 10% of the BSM's field (Figure 2-5, Figure 2-7, and Figure 2-8). In contrast, both plate flexure theory [Turcotte and Schubert, 2001] and thin-plate finite-strain theory [e.g., Seth, 1935] predict plate bending stresses that are of the order of several 100 MPa — 1 GPa over mantle-convection time-scales. Therefore, the ESPM (as well as the BSM) introduces stress perturbations during the seismic cycle that are much smaller than the long-term stress field associated with plate tectonics. Thus, as Savage [1996] argued for the BSM, when this plate-tectonic stress field is added back to that for the BSM, the correct sense of absolute stress is restored all along the bottom of the overriding plate.

The flexural fields discussed in the previous sections help counter the bending strain perturbation from the ESPM, either partially or in full. The key to estimating the ESPM plate thickness,  $H$ , then is identifying what fraction of the flexural stresses associated with the above perturbation is released episodically in the shallow part of the subduction zone. If we can estimate a plate thickness from interseismic geodetic data ignoring this fraction — that is, assume that all of the flexural stresses are only released episodically in the shallow portion of the subduction zone — then we will end up with the minimum

effective plate thickness required by such data. Otherwise, this fraction can also be estimated as an additional ESPM parameter during inversion. Thus, depending on whether other kinds of data warrant the determination of a fractional flexural stress release ( $f_\sigma$ ), the ESPM can be used for inverting interseismic geodetic data with only one ( $H$ ), or two ( $H$ , and  $f_\sigma$ ) additional parameters compared to the BSM.

## 2.7 Discussion

Our capacity to resolve between the BSM and the ESPM, and therefore, the characteristics of plate flexural stress relaxation, depends on whether there are geodetic observations close to the trench [ $x_{GPS} < x_{lock}$ , see Figure 2-1]. Typically, GPS stations are on the overriding plate at distances much larger than  $x_{lock}$  from the trench, where both the ESPM and the BSM predict nearly identical velocities. However, if highly accurate vertical geodetic data are available on the surface of the overriding plate, at distances less than  $x_{lock}$  from the trench — and if we are confident that this data reflects elastic processes — then we would be able to discriminate between the surface deformation fields predicted by these two models if: (a) subducting plate thickness in the ESPM is large, and/or (b) the plate geometry has a large curvature near the trench, and (c) if the volumetric strain associated with plate bending is released episodically in the shallow portions of the subduction zone (< 100 km depth). Even in this case, there will be a trade-off between the actual plate thickness and the fraction of flexural stresses released episodically in the shallow portion of the subduction zone. Therefore, we will only be able to estimate a minimum plate thickness from even a very accurate and dense network of geodetic observation stations. However, if the flexural strain is released continuously in the shallow parts of the subduction zone, or released at larger than  $\sim 100$  km depth — in which case the release occurs too deep to have an effect on the surface deformation of the overriding plate — then the surface velocity fields predicted by the ESPM and the BSM are nearly identical to each other and the latter may be a better model to use because it has two fewer parameters to estimate.

Potential areas where the subduction zone geometry is favorable for testing the ESPM include: Nankai Trough underneath Kii Peninsula [e.g., Hacker et al., 2003 (Figure 3)], Costa Rica Trench, south of the Nicoya peninsula [e.g., Hacker et al., 2003 (Figure 4)], Peru-Chile Trench from Ecuador through Peru [e.g., Gutscher et al., 2000 (Figures 3, 5, and 10)], northern Chile [e.g., ANCORP Working Group, 2003 (Figure 7)], and perhaps, Sumatra [e.g., Chlieh et al., 2008a].

Based on the typical radius of curvature of most subducting slabs, the current distribution of geodetic observations as well as their accuracy, and the surface velocity field predictions above, the ESPM is a relevant model for subduction zones wherever  $H/D_{lock} \geq 2$  — that is, either the locked zone is constrained to be shallow (for instance, from thermal modeling [Oleskevich et al., 1999]) or the downgoing slab can be inferred to be thick (say  $> 50$  km) based on sea-floor age at the trench [e.g., Fowler, 1990; Turcotte and Schubert, 2001]. In contrast, the ESPM with  $H/D_{lock} \leq 1$  is indistinguishable from the BSM, even though the latter may over-predict the extent of the locked zone by roughly 10 km (leading to similar discrepancies in  $x_{lock}$ ); in this case, the BSM may be a better model to use because of its simplicity. These requirements immediately exclude the following: Nankai Trough (because of the small curvature of the Phillipine Sea plate, with shallow dip  $< 15^\circ$  [Park et al., 2002]), Tohoku, Japan Trench (inferred to have very deep locking depth [Suwa et al., 2006]); and Sumatra (because the inferred locking depth is not shallow (30–55 km [Subarya et al., 2006])). The most promising of the above subduction zones for future investigations to discriminate the ESPM from the BSM (or the pBSM) are: Nicoya peninsula, Costa Rica (shallow seismogenic zone and strong slab curvature [DeShon et al., 2006]); and Northern Chile in the vicinity of the Mejillones peninsula (possibly shallow locking depth, and strong plate curvature [ANCORP Working Group, 2003; Brudzinski and Chen, 2005]). Of course if ocean bottom geodetic stations are successfully installed in the future [see for instance, Gagnon et al., 2005], then many of the above subduction zones might be more amenable to application of the ESPM.

To the extent that net deformation remaining after a seismic cycle may contribute incrementally to the long term surface topography of the overriding plate, Figure 2-8(a) (middle panel) points to another important consequence of elastic plate flexure. For a realistic curved subduction megathrust interface, the peak in the vertical surface velocity field due to plate flexure has a magnitude of  $< 5\%$  of the long-term plate convergence rate (for plate thickness of  $< 100$  km), and occurs at distances of approximately 75–150 km arcward of the trench. The location of the peak uplift rate is independent of the plate thickness, but depends strongly on plate curvature. The purely elastic ESPM cannot accumulate such long-term inelastic strain, but it can still provide a measure of where such deformation could occur in the overriding plate over several seismic cycles. In the real Earth, we expect such runaway elastic deformation to be continuously modulated by gravity, inelasticity, accretion, sedimentation, and erosion, resulting in near-equilibrium surface topography. So, if even a small fraction of this peak surface uplift rate arising from elastic flexure promotes inelastic deformation in the real earth, then stable islands, or coastal uplift [e.g., Klotz et al., 2006] could occur at such distances over the long-term. We illustrate this flexural effect for the Sumatran subduction zone (Figure 2-9, with interface geometry as described in [Hsu et al., 2006]). The location of the peak uplift rate is at a distance of  $\sim 100$  km, irrespective of plate thickness (bottom panel of Figure 2-9), and corresponds roughly to the location of the islands in the forearc — as discerned by the along-strike averaged, trench perpendicular bathymetric profile (middle panel of Figure 2-9).

Thus, plate bending could be a plausible driving mechanism for forearc uplift phenomena — such as the presence of forearc islands or coastal uplift — in young, evolving subduction zones, even if only a fraction of the flexural strain after each seismic cycle is inelastic. While such forearc uplift phenomena have been predicted by layered elastic-over viscoelastic models [e.g., Sato and Matsu'ura, 1988; Matsu'ura and Sato, 1989; Sato and Matsu'ura, 1992; 1993; Fukahata and Matsu'ura, 2006], they include many more parameters related to erosion, accretion, and sedimentation, with much larger uncertainties. In addition, the long-term deformation in these models was shown by the above authors to be entirely attributable to only the portion of the fault interface

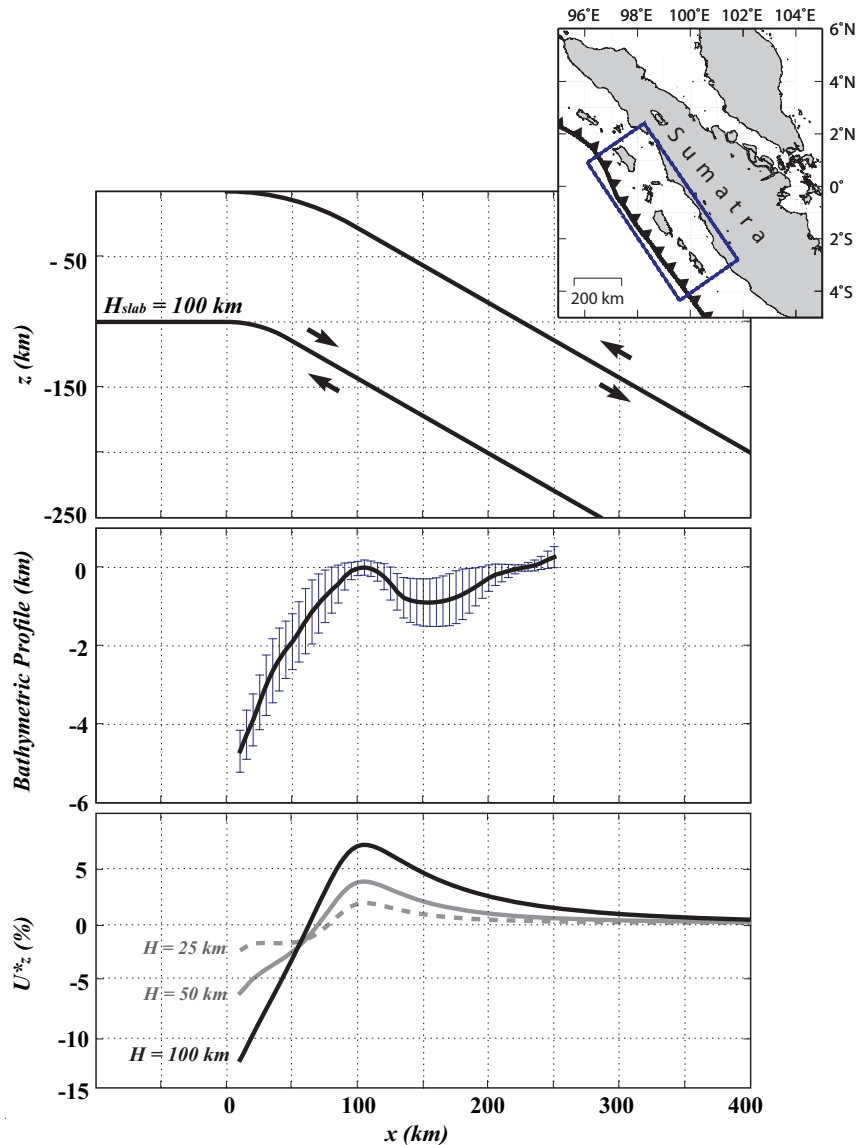


**Figure 2-9.** Comparison of predicted surface velocity profiles from the elastic plate bending flexural field [bottom panel, for plate thicknesses of 25 (dashed gray), 50 (gray), and 100 km (black)], with that of the long-term along-strike averaged trench-perpendicular topographic profile (middle panel, with error bars in blue) for the Sumatran subduction zone (top panel, and inset map). Note that the location of the peak uplift-rate is independent of plate thickness,  $H_{slab}$  (bottom panel). The trench profile in the map is from Bird [2003], and the rectangle indicates the zone of along-strike averaging of the plate geometry (top panel) as well as bathymetry (middle panel). The geometry of the mean plate interface profile (top panel, only  $H_{slab}=100$  km is shown) is similar to that assumed in [Hsu et al., 2006], and attains a dip of  $30^\circ$  at a depth of  $\sim 27$  km below the islands. Note the correspondence in the location of the peak values in the middle and bottom panels. See text for details.



embedded in the upper elastic layer (of thickness  $H$ ), which results in a surface deformation field that is qualitatively similar to that of the steady state component of the ESPM with plate thickness,  $H$ . The advantage of the ESPM is that only a single parameter ( $f_\sigma$ ) is required to determine the potential locations of permanent deformation, and therefore much more conducive to geodetic inversions.

## 2.8 Conclusions

The ESPM can be thought of as a kinematic proxy for slab-buoyancy-driven subduction. The derivation of the ESPM provides a kinematically consistent and physically more intuitive rationale for why the BSM works so well for interpreting current interseismic geodetic data, especially for young, evolving subduction zones. The BSM can be viewed as an end-member model of the ESPM, in the limiting case of zero plate thickness. The BSM is also an end-member model of the ESPM having a finite plate thickness, if all of the stresses associated with these plate flexural strains are either released continuously in the shallow portion of the subduction zone, or released deeper in the subduction zone ( $> 100$  km depth). So, the current practice of fitting available interseismic geodetic data using the BSM is in effect using the ESPM, but assuming either (a) a negligible elastic plate thickness, or (b) that all flexural stresses are released continuously during bending or at depth. Only in the case where these plate flexural stresses are not released continuously in the shallow parts of the subduction zone, can the deformation field of the ESPM be distinguished from that of the BSM. In this case, the differences between the surface velocity fields predicted by the two models is measurable within a few locking depths of the trench, and our ability to discriminate between them is limited by lack of geodetic observations above the locked patch in most subduction zones.

Unlike the pBSM, the ESPM, by definition, yields the correct sense and magnitude of horizontal velocities on the surface of the downgoing plate before it subducts into the trench, as well as zero net steady state block uplift of the overriding plate — primarily because volume conservation is integral to its formulation. Therefore, unlike the pBSM,

the ESPM does not require *ad hoc* steady state velocity corrections. The ESPM eliminates ambiguities associated with the application of the pBSM to non-planar geometries by providing a kinematically consistent framework in which to do so. For plates with curved geometry, the equivalent BSM should have backslip applied along the corresponding curved subduction interface (Figure 2-3, and as explicitly stated by Savage [1983]), and not along the tangent plane to this curved interface at depth.

Characterizing the ESPM requires the estimation of at most two additional parameters (plate thickness, and fraction of flexural stresses released), which can potentially be inverted for in subduction zones that have an  $H/D_{lock}$  ratio equal to 2 or greater. If we assume all flexural stresses are only released episodically in the shallow part of the subduction zone, then this elastic thickness is a minimum plate thickness over the seismic-cycle timescale — as seen by geodetic data. If the BSM is used for the inversion instead of the ESPM, it would predict a wider locked zone compared to the ESPM, assuming that the fault geometry is well constrained. In order to discriminate between the ESPM and the BSM, we must use both the horizontal and vertical surface velocity fields. As the data quality, duration, and coverage improve in the future — especially station density near the trench, say with the deployment of GPS stations on islands or peninsulas close to the trench or on the ocean bottom — inversion for the ESPM parameters can provide an independent estimate for a minimum elastic thickness of the subducting plate, and perhaps even its along-strike variation.

**Table 2-1.** Notation

$\epsilon_{xz}$	Shear-strain
$d\epsilon_{xz}/dt$	Shear strain rate
$\theta, \theta_{dip}$	Planar fault/plate interface dip
$\theta_{bot}$	Dip at the bottom of the locked zone for a curved plate interface
$\Delta\theta$	Change in interface dip from one curved segment to the next
$D_{lock}, d_{lock}$	Depth of locking along the megathrust interface
$C_p$	Local curvature of the centerline of the plate
$f_\sigma$	Fraction of flexural stresses released episodically at shallow depths
$H$	Thickness of the subducting plate in the ESPM
$R_{bot}$	Local radius of curvature for the bottom surface of the plate
$R_p$	Local radius of curvature for the centerline of the plate
$R_{top}$	Local radius of curvature for the top surface of the plate
$s$	Arc-length along the plate interface, or fault-width
$s_{lock}$	Width of locked plate interface
$T_e$	Elastic plate thickness in plate flexure models
$\delta V$	Velocity perturbation to be added to (subtracted from) the centerline plate velocity
$V_{bot}$	Velocity at the bottom surface of the plate
$V_p$	Plate convergence velocity
$V_{top}$	Velocity at the top surface of the plate
$V_x^*$	Horizontal surface velocity normalized by plate rate
$V_z^*$	Vertical surface velocity normalized by plate rate
$x$	Horizontal coordinate, positive landward, or away from the trench
$x^*$	Horizontal coordinate, normalized w.r.t. locking depth
$x_{GPS, (min/max)}$	Distance range from the trench to the nearest geodetic observation
$x_{hinge}$	Distance from the trench to the location of zero vertical surface velocity
$x_{lock}$	Distance between trench and surface projection of the downdip end of the locked zone
$x_{max}$	Distance from trench to the location of the peak in the vertical surface velocity field
$z$	Vertical coordinate, positive upward (depths are therefore, negative)
$z^*$	Vertical coordinate, normalized w.r.t. locking depth

## References

- ANCORP-Working-Group (2003), Seismic Imaging of a convergent continental margin and plateau in the central Andes (Andean Continental Research Project 1996 (ANCORP'96)), *J. Geophys. Res.*, 108, B7, 10.1029/2002JB001771.
- Bird, P. (2003), An updated digital model of plate boundaries, *Geochem Geophys Geosy*, 4, 3, 1027, doi:10.1029/2001GC000252.
- Brudzinski, M. R., and Chen, W.-P. (2005), Earthquakes and strain in subhorizontal slabs, *J. Geophys. Res.*, 110, B08303, 10.1029/2004JB003470.
- Buffett, B. A. (2006), Plate force due to bending at subduction zones, *J. Geophys. Res.*, 111, B9, B09405, [10:1029/2006JB004295](https://doi.org/10.1029/2006JB004295).
- Chlieh, M., Avouac, J.-P., Sieh, K., Natawidjaja, D. H., and Galetzka, J. (2008), Heterogeneous coupling on the Sumatra megathrust constrained from geodetic and paleogeodetic measurements, *J. Geophys. Res.*, 113, B05305.
- Chlieh, M., Chabalier, J. B. d., Ruegg, J. C., Armijo, R., Dmowska, R., Campos, J., and Feigl, K. L. (2004), Crustal deformation and fault slip during the seismic cycle in the North Chile subduction zone, from GPS and InSAR observations, *Geophys. J. Int.*, 158, 2, 695-711, 10.1111/j.1365-246X.2004.02326.x
- Cohen, S. C. (1999), Numerical Models of Crustal Deformation in Seismic Zones, *Adv. Geophys.*, 41, 133-231.
- Conrad, C. P., and Hager, B. H. (1999), Effects of plate bending and fault strength at subduction zones on plate dynamics, *J. Geophys. Res.*, 104, 17551-17571.
- DeShon, H. R., Schwartz, S. Y., Newman, A. V., González, V., Protti, M., Dorman, L. M., Dixon, T. H., Sampson, D. E., and Flueh, E. R. (2006), Seismogenic zone structure beneath the Nicoya Peninsula, Costa Rica, from three-dimensional local earthquake P- and S-wave tomography, *Geophys. J. Int.*, 164, 1, 109–124.
- Elsasser, W. M. (1971), Sea-floor spreading as thermal convection, *J. Geophys. Res.*, 76, 1101-1112.
- Forsyth, D. W., and Uyeda, s. (1975), On the relative importance of the driving forces of plate motion, *Geophys. J. R. Astron. Soc.*, 43, 163-200.
- Fowler, C. M. R. (1990), *The solid earth*, 472 pp., Cambridge University Press, Cambridge.

- Freund, L. B., and Barnett, D. M. (1976), A Two-Dimensional Analysis of Surface Deformation due to Dip-slip Faulting, *Bull. Seismol. Soc. Am.*, 66, 3, 667-675.
- Gagnon, K., Chadwell, C. D., and Norabuena, E. (2005), Measuring the onset of locking in the Peru–Chile trench with GPS and acoustic measurements, *Nature*, 434, 205–208.
- Gutscher, M.-A., Spakman, W., Bijwaard, H., and Engdahl, E. R. (2000), Geodynamics of at subduction: Seismicity and tomographic constraints from the Andean margin, *Tectonics*, 19, 5, 814-833.
- Hacker, B. R., Peacock, S. M., Abers, G. A., and Holloway, S. D. (2003), Subduction Factory, 2: Are intermediate-depth earthquakes in subducting slabs linked to metamorphic dehydration reactions?, *J. Geophys. Res.*, 108, B1, 2030, 10.1029/2001JB001129.
- Hager, B. H. (1984), Subducted slabs and the geoid: constraints on mantle rheology and flow. , *J. Geophys. Res.*, 89, 6003-6015.
- Heki, K. (2004), Space Geodetic Observation of Deep Basal Subduction Erosion in Northeastern Japan, *Earth Planet. Sci. Lett.*, 219, 13-20.
- Hsu, Y.-J., Simons, M., Avouac, J.-P., Galetzka, J., Sieh, K., Chlieh, M., Natawidjaja, D., Prawirodirdjo, L., and Bock, Y. (2006), Frictional Afterslip Following the 2005 Nias-Simeulue Earthquake, Sumatra, *Science*, 312, 5782, 1921-1926, 10.1126/science.1126960.
- Iio, Y., Sagiya, T., and Kobayashi, Y. (2004), Origin of the Concentrated Deformation Zone in the Japanese Islands and Stress Accumulation Process of Intraplate earthquakes, *Earth Planets Space*, 56, 831-842.
- Iio, Y., Sagiya, T., Kobayashi, Y., and Shiozaki, I. (2002), Water-weakened lower crust and its role in the concentrated deformation in the Japanese Islands, *Earth Planet. Sci. Lett.*, 203, 245-253.
- Kanamori, H., and Anderson, D. L. (1975), Theoretical basis of some empirical relations in seismology, *Bull. Seism. Soc. Am.*, 65, 1073-1095.
- Klotz, J., Abolghasem, A., Khazaradze, G., Heinze, B., Vietor, T., Hackney, R., Bataille, K., Maturana, R., Viramonte, J., and Perdomo, R. (2006), Long-term signals in the present-day deformation field of the Central and Southern Andes and Constraints on the viscosity of the Earth's Upper Mantle. , in *The Andes: Active Subduction Orogeny*, *Frontiers in Earth Sciences*, edited by O. Oncken, G. Chong, G. Franz, P. Giese, H. Goetze, V. A. Ramos, M. R. Strecker and P. Wigger, pp. 65–89, Springer Berlin.
- Masterlark, T. (2003), Finite element model predictions of static deformation from dislocation sources in a subduction zone: Sensitivities to homogeneous, isotropic, Poisson-solid, and half-space assumptions, *J. Geophys. Res.*, 108 B11, 2540, 10.1029/2002JB002296.

- Nishimura, T., Hirasawa, T., Miyazaki, S., Sagiya, T., Tada, T., Miura, S., and Tanaka, K. (2004), Temporal change of interplate coupling in northeastern Japan during 1995-2002 estimated from continuous GPS observations, *Geophys. J. Int.*, 157, 901-916.
- Okada, Y. (1992), Internal deformation due to shear and tensile faults in a half-space, *Bull. Seismol. Soc. Am.*, 82, 2, 1018-1040.
- Oleskevich, D. A., Hyndman, R. D., and Wang, K. (1999), The updip and downdip limits to great subduction earthquakes: thermal and structural models of Cascadia, south Alaska, SW Japan, and Chile, *J. Geophys. Res.*, 104, 14965–14991.
- Park, J.-O., Tsuru, T., Kodaira, S., Cummins, P. R., and Kaneda, Y. (2002), Splay Fault Branching Along the Nankai Subduction Zone, *Science*, 297, 1157-1160.
- Rani, S., and Singh, S. J. (1992), Static Deformation of a Uniform Half-space due to a Long Dip-slip Fault, *Geophys. J. Int.*, 109, 469-476.
- Savage, J. C. (1983), A dislocation model of strain accumulation and release at a subduction zone, *J. Geophys. Res.*, 88 4984-4996.
- Savage, J. C. (1995), Interseismic uplift at the Nankai subduction zone, Southwest Japan, 1951–1990, *J. Geophys. Res.*, 100, 6339–6350.
- Savage, J. C. (1996), Comment on "The stress state implied by dislocation models of subduction deformation" by J. J. Douglass and B. A. Buffett, *Geophys. Res. Lett.*, 23, 19, 2709-2710.
- Savage, J. C. (1998), Displacement field for an edge dislocation in a layered half-space, *J. Geophys. Res.*, 103, 2439-2446.
- Seth, B. R. (1935), Finite Strain in Elastic Problems, *Philosophical Transactions of the Royal Society of London*, 234, 738, 231-264.
- Sieh, K., Ward, S. N., Natawidjaja, D., and Suwargadi, B. W. (1999), Crustal deformation at the Sumatran subduction zone revealed by coral rings, *Geophys. Res. Lett.*, 26, 3141-3144.
- Souter, B. J., and Hager, B. H. (1997), Fault propagation fold growth during the 1994 Northridge, California, earthquake?, *J. Geophys. Res.*, 102, B6, 11,931–911,942.
- Subarya, C., Chlieh, M., Prawirodirdjo, L., Avouac, J. P., Bock, Y., Sieh, K., Meltzner, A., Natawidjaja, D., and McCaffrey, R. (2006), Plate-boundary deformation of the great Aceh-Andaman earthquake, *Nature*, 440, 46–51.
- Suppe, J. (1985), *Principles of Structural Geology*, 537 pp., Prentice-Hall.

- Suwa, Y., Miura, S., Hasegawa, A., Sato, T., and Tachibana, K. (2006), Interplate coupling beneath NE Japan inferred from three-dimensional displacement field, *J. Geophys. Res.*, 111, B4, B04402, 10.1029/2004JB003203.
- Tomar, S., and Dhiman, N. K. (2003), 2D Deformation Analysis of a Half-space due to a Long Dip-slip Fault at Finite Depth, *Proc. Indian Acad. Sci. (Earth Planet. Sci.)*, 112, 4, 587-596.
- Turcotte, D. L., and Schubert, G. (2001), *Geodynamics*, 2 ed., 456 pp., Cambridge University Press, New York.
- Twiss, R. J., and Moores, E. M. (1992), *Structural Geology*, 1st ed., 532 pp., W. H. Freeman and Company, New York.
- Vergne, J., Cattin, R., and Avouac, J. P. (2001), On the use of Dislocations to Model Interseismic Strain and Stress Build-up at Intracontinental Thrust Faults, *Geophys. J. Int.*, 147, 1, 155-162, 10.1046/j.1365-246X.2001.00524.x.
- Wang, K. (2007), Elastic and viscoelastic models of crustal deformation in subduction earthquake cycles, in *The Seismogenic Zone of Subduction Thrust Faults*, edited by T. Dixon and J. C. Moore, pp. 540-575, Columbia University Press, New York.
- Wang, K., and Hu, Y. (2006), Accretionary Prisms in Subduction Earthquake Cycles: The Theory of Dynamic Coulomb Wedge, *J. Geophys. Res.*, 111, B06410, 10.1029/2005JB004094.
- Wang, R. (2005), The dislocation theory: a consistent way for including the gravity effect in (visco)elastic plane-earth models, *Geophys. J. Int.*, 161, 191-196.
- Yoshioka, S., Yabuki, T., Sagiya, T., Tada, T., and Matsu'ura, M. (1993), Interplate coupling and relative plate motion in the Tokai district, central Japan, deduced from geodetic data inversion using ABIC, *Geophys. J. Int.*, 113, 607-621.
- Zhao, S., and Takemoto, S. (2000), Deformation and stress change associated with plate interaction at subduction zones: a kinematic modeling, *Geophys. J. Int.*, 142, 300-318.